

---

# Emulating the Global Change Analysis Model with Deep Learning

---

Andrew Holmes<sup>1</sup>, Matt Jensen<sup>2</sup>, Sarah Coffland<sup>1</sup>, Hidemi Mitani Shen<sup>1</sup>, Logan Sizemore<sup>1</sup>,  
Seth Bassetti<sup>3</sup>, Brenna Nieva<sup>1</sup>, Claudia Tebaldi<sup>4</sup>, Abigail Snyder<sup>4</sup>, Brian Hutchinson<sup>1,4</sup>

<sup>1</sup> Computer Science Dept, Western Washington University, Bellingham, WA, USA

<sup>2</sup> Applied Artificial Intelligence Systems, Pacific Northwest National Laboratory, Seattle, WA, USA

<sup>3</sup> Computer Science Department, Utah State University, Logan, UT, USA

<sup>3</sup> Utah State University, Logan, UT, USA

<sup>4</sup> Joint Global Change Research Institute, Pacific Northwest National Laboratory, College Park, MD

## Abstract

The Global Change Analysis Model (GCAM) simulates complex interactions between the coupled Earth and human systems, providing valuable insights into the co-evolution of land, water, and energy sectors under different future scenarios. Understanding the sensitivities and drivers of this multisectoral system can lead to more robust understanding of the different pathways to particular outcomes. The interactions and complexity of the coupled human-Earth systems make GCAM simulations costly to run at scale - a requirement for large ensemble experiments which explore uncertainty in model parameters and outputs. A differentiable emulator with similar predictive power, but greater efficiency, could provide novel scenario discovery and analysis of GCAM and its outputs, requiring fewer runs of GCAM. As a first use case, we train a neural network on an existing large ensemble that explores a range of GCAM inputs related to different relative contributions of energy production sources, with a focus on wind and solar. We complement this existing ensemble with interpolated input values and a wider selection of outputs, predicting 22, 528 GCAM outputs across time, sectors, and regions. We report a median  $R^2$  score of 0.998 for the emulator's predictions and an  $R^2$  score of 0.812 for its input-output sensitivity.

## 1 Introduction and Background

The global change problem involves both Earth and human system dynamics, interacting and creating feedbacks among the multiple components and sectors that make up the whole system. The Global Change Analysis Model (GCAM) [2, 3] and other models of the same class are essential to represent the future evolution of the human system, including socioeconomic, land, energy, and water sectors, giving rise to future plausible and coherent scenarios of emissions. These scenarios are in turn used as drivers of Earth system model projections. In the opposite direction, climate output from Earth system models is used to model impacts in GCAM and other integrated multi-sector models. This work focuses on emulating GCAM specifically; it is an open-source multisector dynamic model that simulates the integrated, simultaneous evolution of energy, agriculture, land use, water, and climate system components. GCAM simulates global markets segmented into 32 distinct socioeconomic regions, 235 hydrological basins, forming 384 land units from the intersection of basins and regions.

Historically, GCAM and comparable models have run a discrete set of “storylines” or representative future scenarios. In contrast, thanks to advances in computational power and analysis tools, exploratory modeling, sampling a much larger set of drivers (and therefore outcomes) has become popular in recent years [4, 5]. In this approach, large ensembles of scenarios are designed and run

to fill the gaps between the representative storyline scenarios. This approach has been fruitful for exploring the complex sensitivities these models have to assumptions about the systems under test, and the external drivers that determine their outcomes. This understanding of sensitivity and drivers can facilitate identification of pros and cons of different pathways to outcomes of interest (e.g., to minimize water scarcity [5]). The ensembles are often designed to incorporate a range of data sources, expert opinion, and discrete parameterizations in a factorial combination [18]. However, even with access to modern computing clusters, computational cost hinders a comprehensive exploration of these inputs. We aim to enable this comprehensive exploration via deep learning-based emulation of GCAM. Existing large ensembles provide data to train and evaluate such emulators.

Once trained, a high-fidelity emulator can be used to aid our understanding both of the coupled Earth-human systems and their models (e.g., GCAM). For example, an emulator could be used to explore the input (assumption) space, to steer the generation of large GCAM ensembles, or to better characterize model sensitivities. There are two defining aspects to our approach that set it apart from GCAM toward these goals. First, once trained, predicting outcomes for novel scenarios is faster than GCAM by at least three orders of magnitude. Second, the differentiability of the emulation enables efficient search algorithms over the input space. Relatively little work has been done with emulation of integrated, multisector models, but results have been promising [17, 19]. Here we introduce a high-fidelity emulator of GCAM, both in the predictions and in the input-output sensitivities.

## 2 Methods

### 2.1 Data

Each scenario of GCAM is shaped by exogenous factors like socioeconomic trends (population and GDP growth), technology costs and performance, historical information, and assumptions about future values of key drivers. These are what we call “inputs” in this paper, and a subset of these will be sampled in our ensembles. GCAM provides a detailed, time-evolving analysis of sectors within the economy and simulates how different external factors might affect specific sectors over time, taking into account the effects from all other sectors; these serve as the outputs of our emulator.

**Inputs:** This paper follows the experiment set up by Woodard et al. [18], W2023 henceforth, to study the effect of varying inputs on wind and solar energy adoption by 2050. We use the same 12 GCAM inputs as W2023, representing costs, constraints, backups, and demand in the energy sector. These factors were chosen by climate experts to describe a wide variety of scenarios to explore GCAM and its outputs. Table 2 describes each of the 12 inputs. In W2023 experiments, these factors were held to *high* and *low* values which were encoded as 1 and 0, respectively, in our experiments.

To enrich the input space, we consider here input values between the high and low. For nine of the 12 inputs (see Appendix A), an *intermediate* value between high and low is well-defined, so we relax the domain from  $\{0, 1\}$  to the interval  $0 \leq x \leq 1$ . The extreme high and low values still represent the original binary meaning, while all intermediate values are linearly interpolated between the high and low scenarios. For three of the twelve inputs, a notion of *intermediate* is not well-defined; namely, for bioenergy, electrification, and emissions, the binary values represent the presence of absence of specific input files to GCAM.

**Sampling Strategies:** With the introduction of interpolated values, the input space can no longer be enumerated, so we consider two strategies for sampling the space: Latin hypercube [12] and “finite-diff” [15, 16]. In either strategy, the nine interpolated inputs are sampled by the strategy while the remaining three inputs are randomly sampled uniformly in  $\{0, 1\}$ . We selected Latin hypercube to efficiently explore the interpolated input space, while the finite-diff was selected to support our sensitivity analysis. We sample 4096 input configurations for Latin hypercube data (denoted here “interpolated”) data, which we split into training, validation and test sets at an 80%/10%/10% ratio. The finite-diff data (denoted here as the “DGSM” or “sensitivity” dataset) contains 4000 samples and is entirely test set, as it was used neither for model training nor tuning.

**Outputs:** Each GCAM run produces a large output database related to the energy, water, climate, and land sectors. Among these, we identify 44 GCAM output quantities to predict (see Appendix B for full details). These quantities were chosen to cover physical quantities and prices over the major

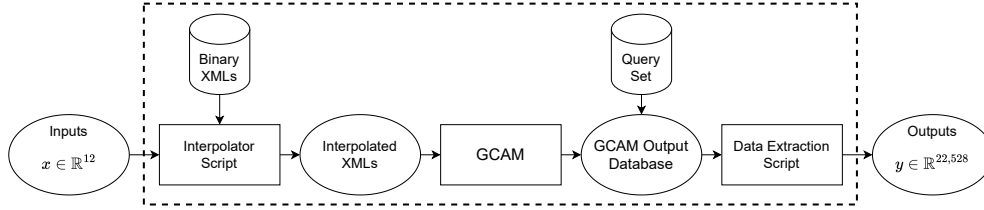


Figure 1: Diagram of the input-output relationship using GCAM. The emulator approximates the dashed box, mapping directly from inputs to outputs

resources in the water, land, and energy sectors relevant to renewable energy adoption, in light of the focus in W2023. For each of the 44 output quantities, GCAM and our emulator predict values over 32 regions and over 16 model years,  $\{2025, 2030, 2035, \dots, 2095, 2100\}$ . This yields a total output dimension of 22,528 values to predict.

## 2.2 Emulator

Figure 1 illustrates the emulation problem. Our emulator abstracts a series of steps between inputs and outputs, including interpolating the configuration XMLs, running GCAM, and running queries to extract the output values of interest.

**Model Architecture:** Motivated by the success of neural networks learning non-linear relationships [7], we employ a neural network to emulate input-output relationship (dashed box of Fig. 1). Specifically, we use a four-layer, feed-forward, fully connected neural network, each layer with 256 hidden units followed by a linear rectified unit (ReLU) hidden activation function [6]. The fully connected output layer contains 22,528 units.

**Training:** The model is trained to minimize mean squared error loss between the emulator predictions and GCAM outputs on the training set using hyperparameters selected with a Bayesian Hyperparameter search [14] via Weights and Biases [1] on the validation set. All output values are z-score normalized using their training set statistics – each quantity-region-year pair  $x_{qry}$  is normalized using  $(x_{qry} - \mu_{qry})/\sigma_{qry}$ ; where mean ( $\mu_{qry}$ ) and standard deviation ( $\sigma_{qry}$ ) are computed for that specific quantity-region-year value across all training dataset scenarios. We train with the AdamW [11] stochastic optimization algorithm for 500 epochs with a learning rate of 0.001.

## 3 Results and Analysis

As summarized in Table 1, we analyze the performance of our emulator by comparing the output values to those of GCAM, as well as comparing the sensitivities of the emulator to those of GCAM. For the “Predictions” row of the table, we evaluate the “Overall” emulator performance on the interpolated test set by calculating the  $R^2$  score for each of the 22,528 output values and report the median over these output values. This shows very high agreement with GCAM, with a median  $R^2$  of 0.998. The results for Region, Year, and Quantity involve first aggregating targets over the other two dimensions (e.g., Region averages over Year and Quantity);  $R^2$  is then computed for each the remaining outputs (44 if Quantity, 32 if Region, 16 if Year), and the median  $R^2$  over these aggregated outputs is reported. This level of aggregation does not improve the already near-perfect overall  $R^2$ .

Table 1: Evaluation of emulator on test sets. Results are reported as  $R^2$  values between GCAM and the emulator on its predictions (on the interpolated test set) and on input-output DGMS sensitivity (on the DGSM set), aggregated to region, year or quantity-level, and overall (no aggregation).

	Region	Year	Quantity	Overall
Predictions	0.998	0.998	0.998	0.998
Sensitivity	0.989	0.990	0.995	0.812

To further evaluate the quality of the emulator, we perform a Derivative-based Global Sensitivity Measure (DGSM) analysis [16], as implemented in the SALib package [8, 9], on both our emulator and on GCAM. Specifically, we compare  $S_{ij}^\sigma$  values defined as follows:

$$S_{ij}^\sigma = \frac{\sigma_{x_i}}{\sigma_{y_j}} S_{ij}, \text{ where } S_{ij} = \mathbb{E} \left[ \left( \frac{\partial y_j}{\partial x_i} \right)^2 \right].$$

$S_{ij}$  is the  $\nu$  value from [16], while  $\sigma_z$  denotes the standard deviation of  $z$ .  $S_{ij}^\sigma$  is a normalized version of  $S_{ij}$ ; normalizing this way better captures the true effect of input  $x_i$  on output  $y_j$  [13], given the wide range of magnitudes and units in GCAM inputs and outputs. The sensitivity analysis uses the DGSM dataset, generated with the finite-diff sampling strategy; sensitivities are calculated by observing the effects of introducing small perturbations around each input parameter and seeing how each of the outputs respond. For the emulator and for GCAM, we calculate  $S_{ij}^\sigma$  for all inputs  $x_i$  and outputs  $y_j$ .

The Overall result, summarized in Table 1, is the  $R^2$  agreement between the  $S^\sigma$  matrix for the emulator and the  $S^\sigma$  matrix for GCAM. At 0.812, we observe good agreement between the emulator and GCAM with respect to the input-output sensitivities. For the Region, Year and Quantity breakdowns, we average the  $S^\sigma$  matrices over disjoint subsets of output variables  $j$ , leaving only the specified dimension (e.g., the Quantity breakdown uses  $S^\sigma \in \mathbb{R}^{9 \times 44}$ , having averaged sensitivities over Year and Region). Sensitivity agreement at this coarser resolution is very high, ranging from 0.989 for Region to 0.995 for Quantity.

The input-output sensitivities, both of the emulator and GCAM, yield some interesting trends. Most notably, there is a high normalized sensitivity to the *energy* input factor for many of the outputs. This makes sense because this particular input variable affects the GDP and population assumptions, which past exploratory studies have also found to be the largest contributor to outputs [4, 10]. Predictably, we also see a strong sensitivity to the energy input factor among regions with large economies and high populations, such as China, India, and the USA. Several of the output quantities stand out as highly sensitive to the inputs; in particular, *electricity price* and many land sector outputs. Electricity price reflects the input drivers chosen for this ensemble, which experts selected specifically because they would affect energy prices from different technologies and therefore relative adoption of wind and solar. The land sector has been studied in past analyses [4, 10] showing that the inherently finite nature of land availability for feeding changing populations is often a key determinant of outcomes. See Appendix C for additional information.

## 4 Conclusion and Future Work

We present in this paper a high-fidelity and computationally efficient emulator of GCAM using deep learning. In the process of doing so, we enriched the sampling strategy of inputs underpinning an existing exploration (in W2023) of the drivers of renewable energy deployment by 2050, relaxing 9 of 12 input variables from binary to continuous. This represents a particularly valuable addition to the past study that, by limiting exploration to binary choices for the input parameters, risked overlooking outcomes of interest associated with intermediate values. We confirm that our emulator is highly accurate and that its sensitivities are consistent with GCAM’s. In future work, we plan to explore the use of this high-fidelity emulator for searching over input space (e.g., to identify circumstances that minimize water scarcity) to steer the generation of large ensembles of GCAM, and to better understand GCAM itself. Ultimately, we view this work as a bridge to a new era where large ensembles are still relevant, but their creation can be aided by machine learning to reduce the cost and complexity; future work to answer scientific questions around climate, energy, land and water systems can generate tailored ensembles in an iterative, emulator-in-the-loop manner.

## 5 Acknowledgements

This research was supported by the U.S. Department of Energy, Office of Science, as part of research in MultiSector Dynamics, Earth and Environmental System Modeling Program. The Pacific Northwest National Laboratory is operated for DOE by Battelle Memorial Institute under contract DE-AC05-76RL01830. The views and opinions expressed in this paper are those of the authors alone.

## References

- [1] Lukas Biewald. Experiment tracking with weights and biases, 2020. Software available from wandb.com.
- [2] Ben Bond-Lamberty, Kalyn Dorheim, Ryna Cui, Russell Horowitz, Abigail Snyder, Katherine Calvin, Leyang Feng, Rachel Hoesly, Jill Horing, G. Page Kyle, Robert Link, Pralit Patel, Christopher Roney, Aaron Staniszewski, Sean Turner, Min Chen, Felipe Feijoo, Corinne Hartin, Mohamad Hejazi, Gokul Iyer, Sonny Kim, Yaling Liu, Cary Lynch, Haewon McJeon, Steven Smith, Stephanie Waldhoff, Marshall Wise, and Leon Clarke. Gcamdata: An R Package for Preparation, Synthesis, and Tracking of Input Data for the GCAM Integrated Human-Earth Systems Model. *7(1):6*, March 2019.
- [3] Katherine Calvin, Pralit Patel, Leon Clarke, Ghassem Asrar, Ben Bond-Lamberty, Ryna Yiyun Cui, Alan Di Vittorio, Kalyn Dorheim, Jae Edmonds, Corinne Hartin, Mohamad Hejazi, Russell Horowitz, Gokul Iyer, Page Kyle, Sonny Kim, Robert Link, Haewon McJeon, Steven J. Smith, Abigail Snyder, Stephanie Waldhoff, and Marshall Wise. GCAM v5.1: Representing the linkages between energy, water, land, climate, and economic systems. *Geoscientific Model Development*, 12(2):677–698, February 2019.
- [4] Flannery Dolan, Jonathan Lamontagne, Katherine Calvin, Abigail Snyder, Kanishka B. Narayan, Alan V. Di Vittorio, and Chris R. Vernon. Modeling the Economic and Environmental Impacts of Land Scarcity Under Deep Uncertainty. *Earth's Future*, 10(2):e2021EF002466, February 2022.
- [5] Flannery Dolan, Jonathan Lamontagne, Robert Link, Mohamad Hejazi, Patrick Reed, and Jae Edmonds. Evaluating the economic impact of water scarcity in a changing world. *Nature Communications*, 12(1):1915, March 2021.
- [6] Kunihiko Fukushima. Visual Feature Extraction by a Multilayered Network of Analog Threshold Elements. *IEEE Transactions on Systems Science and Cybernetics*, 5(4):322–333, 1969.
- [7] Ian Goodfellow, Yoshua Bengio, and Aaron Courville. *Deep Learning*. MIT Press, 2016.
- [8] Jon Herman and Will Usher. SALib: An open-source python library for sensitivity analysis. *The Journal of Open Source Software*, 2(9), jan 2017.
- [9] Takuya Iwanaga, William Usher, and Jonathan Herman. Toward SALib 2.0: Advancing the accessibility and interpretability of global sensitivity analyses. *Socio-Environmental Systems Modelling*, 4:18155, May 2022.
- [10] Franklyn Kanyako, Jonathan Lamontagne, Abigail Snyder, Jennifer Morris, Gokul Iyer, Flannery Dolan, Yang Ou, and Kenneth Cox. Compounding uncertainties in economic and population growth increase tail risks for relevant outcomes across sectors. *Earth's Future*, 2023.
- [11] Ilya Loshchilov and Frank Hutter. Decoupled Weight Decay Regularization. 2017.
- [12] M. D. McKay, R. J. Beckman, and W. J. Conover. A Comparison of Three Methods for Selecting Values of Input Variables in the Analysis of Output from a Computer Code. *Technometrics*, 21(2):239, May 1979.
- [13] Andrea Saltelli, Marco Ratto, Terry Andres, Francesca Campolongo, Jessica Cariboni, Debora Gatelli, Michaela Saisana, and Stefano Tarantola. *Global Sensitivity Analysis: The Primer*. Wiley-Interscience, Chichester, England, 2008.
- [14] Jasper Snoek, Hugo Larochelle, and Ryan P Adams. Practical bayesian optimization of machine learning algorithms. 2012.
- [15] I.M Sobol'. Global sensitivity indices for nonlinear mathematical models and their Monte Carlo estimates. *Mathematics and Computers in Simulation*, 55(1-3):271–280, February 2001.
- [16] I.M. Sobol' and S. Kucherenko. Derivative based global sensitivity measures and their link with global sensitivity indices. *Mathematics and Computers in Simulation*, 79(10):3009–3017, June 2009.
- [17] Jun'ya Takakura, Shinichiro Fujimori, Kiyoshi Takahashi, Naota Hanasaki, Tomoko Hasegawa, Yukiko Hirabayashi, Yasushi Honda, Toshichika Iizumi, Chan Park, Makoto Tamura, and Yasuaki Hijioka. Reproducing complex simulations of economic impacts of climate change with lower-cost emulators. *Geoscientific Model Development*, 14(5):3121–3140, June 2021.

- [18] Dawn L. Woodard, Abigail Snyder, Jonathan R. Lamontagne, Claudia Tebaldi, Jennifer Morris, Katherine V. Calvin, Matthew Binsted, and Pralit Patel. Scenario Discovery Analysis of Drivers of Solar and Wind Energy Transitions Through 2050. *Earth's Future*, 11(8):e2022EF003442, August 2023.
- [19] Weiwei Xiong, Katsumasa Tanaka, Philippe Ciais, Daniel J. A. Johansson, and Mariliis Lehtveer. emIAM v1.0: An emulator for Integrated Assessment Models using marginal abatement cost curves. Preprint, Integrated assessment modeling, March 2023.

Table 2: Inputs varied for each run of GCAM. Interpolated inputs in bold.

Input	Key	Description
<b>Wind and Solar Backups</b>	back	Systems needed to backup wind and solar
Bioenergy	bio	Tax on bioenergy
<b>Carbon Capture</b>	ccs	Carbon storage resource cost
Electrification	elec	Share of electricity in building, industry, and transportation
Emissions	emiss	CO <sub>2</sub> emission constraints
<b>Energy Demand</b>	energy	Energy Demand - GDP and population assumptions
<b>Fossil Fuel Costs</b>	ff	Cost of crude oil, unconventional oil, natural gas, and coal
<b>Nuclear Costs</b>	nuc	Capital overnight costs
<b>Solar Storage Costs</b>	solarS	Solar storage capital overnight costs
<b>Solar Tech Costs</b>	solarT	CSP and PV costs
<b>Wind Storage Costs</b>	windS	Wind storage capital overnight costs
<b>Wind Tech Costs</b>	windT	Wind and wind offshore capital overnight costs

### A Inputs (Drivers)

The 12 input variables are described in Table 2.

### B Output Quantities

Our 44 output quantities are described in Table 3.

### C Input-Output Sensitivities

See Figure 2 for sensitivity values.

resource	metric	sector	units	query name
energy	demand_electricity	building	EJ	elec_consumption_by_demand_sector
energy	demand_electricity	industry	EJ	elec_consumption_by_demand_sector
energy	demand_electricity	transport	EJ	elec_consumption_by_demand_sector
energy	demand_fuel	building	EJ	final_energy_consumption_by_sector_and_fuel
energy	demand_fuel	industry	EJ	final_energy_consumption_by_sector_and_fuel
energy	demand_fuel	building	EJ	final_energy_consumption_by_sector_and_fuel
energy	demand_fuel	industry	EJ	final_energy_consumption_by_sector_and_fuel
energy	demand_fuel	transport	EJ	final_energy_consumption_by_sector_and_fuel
energy	price	coal	1975\$/GJ	final_energy_prices
energy	price	electricity	1975\$/GJ	final_energy_prices
energy	price	transport	1975\$/GJ	final_energy_prices
energy	price	transport	1975\$/GJ	final_energy_prices
energy	supply_electricity	biomass	EJ	elec_gen_by_subsector
energy	supply_electricity	coal	EJ	elec_gen_by_subsector
energy	supply_electricity	gas	EJ	elec_gen_by_subsector
energy	supply_electricity	nuclear	EJ	elec_gen_by_subsector
energy	supply_electricity	oil	EJ	elec_gen_by_subsector
energy	supply_electricity	other	EJ	elec_gen_by_subsector
energy	supply_electricity	solar	EJ	elec_gen_by_subsector
energy	supply_electricity	wind	EJ	elec_gen_by_subsector
energy	supply_primary	biomass	EJ	primary_energy_consumption_by_region
energy	supply_primary	coal	EJ	primary_energy_consumption_by_region
energy	supply_primary	gas	EJ	primary_energy_consumption_by_region
energy	supply_primary	nuclear	EJ	primary_energy_consumption_by_region
energy	supply_primary	oil	EJ	primary_energy_consumption_by_region
energy	supply_primary	other	EJ	primary_energy_consumption_by_region
energy	supply_primary	solar	EJ	primary_energy_consumption_by_region
energy	supply_primary	wind	EJ	primary_energy_consumption_by_region
land	allocation	biomass	thousand km2	aggregated_land_allocation
land	allocation	forest	thousand km2	aggregated_land_allocation
land	allocation	grass	thousand km2	aggregated_land_allocation
land	allocation	other	thousand km2	aggregated_land_allocation
land	allocation	pasture	thousand km2	aggregated_land_allocation
land	demand	feed	Mt	demand_balances_by_crop_commodity
land	demand	food	Mt	demand_balances_by_crop_commodity
land	price	biomass	1975\$/GJ	prices_by_sector
land	price	forest	1975\$/m3	prices_by_sector
land	production	biomass	EJ	ag_production_by_crop_type
land	production	forest	billion m3	ag_production_by_crop_type
land	production	grass	Mt	ag_production_by_crop_type
land	production	other	Mt	ag_production_by_crop_type
land	production	pasture	Mt	ag_production_by_crop_type
water	demand	crops	km3	water_withdrawals_by_tech
water	demand	electricity	km3	water_withdrawals_by_tech

Table 3: GCAM outputs quantities with the associated GCAM selection query used to generated the outputs from the GCAM database.



### Derivative-Based Sensitivity Measure

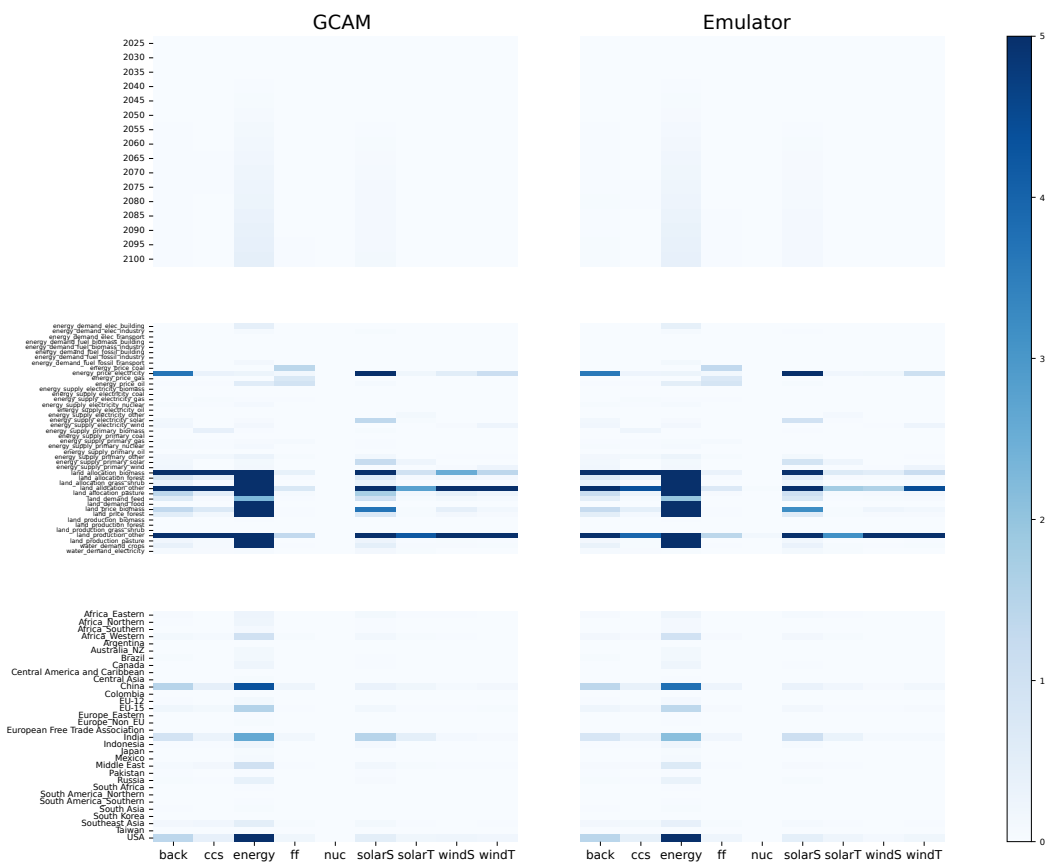


Figure 2: GCAM (left) vs. Emulator (right) local sensitivities of inputs vs Years (Top), Quantities (Middle), and Regions (Bottom).